Indonesian Journal of Data and Science

Volume 7 Issue 2
ISSN 2715-9930
https://doi.org/10.56705/ijodas.v7i2.529

Research Article

Residual-Energy LEACH-PSO Extends Simulated WSN Lifetime under Uneven Node Density

Ramdan Satra [1]; Muhammad Hattah Fattah[2]
[1] Universitas Muslim Indonesia, Makassar, Indonesia, ramdan@umi.ac.id
[2] Universitas Muslim Indonesia, Makassar, Indonesia, muhhattah.fattah@umi.ac.id

Correspondence should be addressed to Ramdan Satra; ramdan@umi.ac.id

Received 24 December 2025; Accepted 12 July 2026; Published 31 July 2026

© Authors 2026. CC BY-NC 4.0 (non-commercial use with attribution, indicate changes).
License: https://creativecommons.org/licenses/by-nc/4.0/ — Published by Indonesian Journal of Data and Science.

Abstract:

Introduction: Uneven spatial node density can concentrate communication burdens in wireless sensor networks (WSNs). This study evaluated the incremental effect of residual-energy cluster-head reassignment on simulated network lifetime. **Method**: LEACH (M1), particle swarm optimization (PSO) seed clustering (M2), and residual-energy LEACH-PSO (M3) were evaluated across 270 synthetic topologies covering nine near–far scenarios with 30 placements each, producing 810 method runs. Every topology contained 200 nodes in a fixed 200 m × 200 m field. M2 and M3 shared radio, traffic, and PSO settings. Within each logical round, M3 retained the PSO-derived membership and selected the member with the highest residual energy after status transmission as cluster head. The primary topology-paired M3–M2 comparison assessed first-node-dead (FND) and half-nodes-dead (HND) rounds using block-bootstrap confidence intervals. **Results and Discussion**: Mean FND and HND were 18.70 and 39.85 rounds for M3, compared with 8.84 and 32.84 for M2. Aggregate paired gains were 9.86 FND rounds (95% CI, 9.44–10.26) and 7.01 HND rounds (95% CI, 6.83–7.19). Both endpoints improved on average in all nine scenarios, with the largest gains when 180 nodes occupied the far zone. No endpoints were censored. **Conclusion**: Cluster-head reassignment based on residual energy extended simulated WSN lifetime under the specified radio and traffic model. Performance under realistic communication conditions and physical deployments requires further validation.

Keywords: Wireless Sensor Networks; LEACH-PSO; Residual-Energy Cluster-Head Selection; Network Lifetime; Uneven Spatial Density; Topology-Paired Simulation.

1. Introduction

Wireless sensor networks combine finite energy reserves, distributed communication, and application-specific traffic, making the allocation of cluster-head work central to modeled network lifetime [1], [2]. LEACH elects cluster heads probabilistically from eligibility-rotated nodes rather than ranking their residual energy [2], [23]; HEED, PEGASIS, and heterogeneous-energy clustering provide contrasting mechanisms for clustering or data gathering [3], [5], [6]. Clustering and energy-conservation surveys identify node location, sink distance, and communication burden as core design dimensions [8]–[10], [24], [25]. Unequal-clustering studies further show why nonuniform geometry and distance to the sink merit explicit treatment [27], [28].

Particle swarm optimization (PSO) is a population-based search mechanism [4]. Here, M2 maps every live node to its nearest PSO seed and retains that seed as cluster head, which need not be the greatest-residual-energy member of its cluster. Earlier WSN studies use PSO to co-design clustering or head choice [7], [9], [26], [29] and unequal multi-hop routing [30], while newer energy-aware protocols combine residual energy with distance, ranking, learning, or mobility [11]–[16]. Because these protocols alter multiple components, they do not identify the incremental effect of one residual-energy head rule.

The novelty here is a controlled, density-stratified test of that incremental rule. First, M2 and M3 have the same prespecified radio model, traffic, PSO budget, topology-specific seed, stopping rule, and seed-based partition procedure. Within a logical round, M2 keeps the PSO seed as head whereas M3 reassigns the fixed membership to the live member with maximum post-status residual energy. A later partition is recomputed from each method's own live set; the study does not claim that memberships remain identical across divergent trajectories. Second, all scenarios retain N = 200, so "uneven density" denotes the spatial near--far distribution, not a change in total network size or a scalability experiment. Third, topology pairing, energy-ledger checks, explicit FND/HND endpoints, bootstrap intervals, and sign-flip inference make the contrast auditable under the stated synthetic model.

2. Method

Study design, terminology, and synthetic topology input

The supplied version-2 archive contains geometry, scenario definitions, a generator, and a validator; it has no observed node-death, cluster-head, or residual-energy outcomes [32]. It was therefore used as synthetic topology input to an executable simulator, not as field evidence. A topology is one coordinate layout; a placement replicate (for example, R01) is one topology generated within a scenario; and a method run is one simulator trajectory for that topology. The nine scenario families and 30 placement replicates per family yielded 270 topologies and 810 method runs.

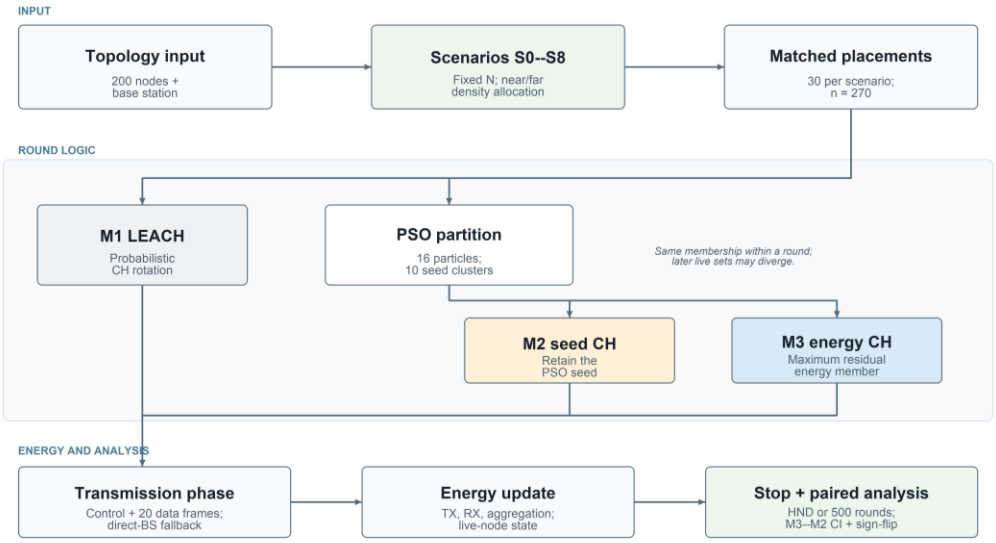


Figure 1. Study workflow for the M1--M3 comparison.

Table 1. Prespecified simulation contract.

Aspect	Prespecified value
Experimental unit	One supplied 200-node synthetic topology; 270 paired topologies
Geometry	200 m × 200 m field; base station (100, 220) m; fixed total N = 200
Methods	M1 probabilistic LEACH; M2 PSO seed as CH; M3 maximum-residual-energy member after the seed partition
Traffic and accounting	20 frames/round; 4,200-bit data; 200-bit control; 0.5 J/node; direct-BS fallback
PSO partition	K = 10; 16 particles; 20 iterations; w = 0.7; c1 = c2 = 1.4; $\|v\| \leq 0.2$
Stopping and analysis	FND/HND; HND or 500-round cap; paired M3−M2 bootstrap, sign-flip, Holm

The field was 200 m × 200 m with the base station at (100, 220) m. Nodes with y >= 100 m were near the base station and those with y < 100 m were far. Table 2 gives every scenario explicitly: both zones have equal 20,000 m² area, total N remains 200, and overall network density therefore remains 5 nodes per 1,000 m². Every node starts at

0.5 J. Input checks found 54,000 nodes, no blank required values, no duplicate node rows, a mean base-station distance of 135.421 m, and a mean 25-m neighbor count of 10.764.

Table 2. Fixed-total-population spatial-density scenarios (near: y >= 100 m; far: y < 100 m).

Scenario	Near nodes	Far nodes	Near:far	Denser zone	Placements
S0	100	100	1:1	Balanced	30
S1	120	80	3:2	Near	30
S2	140	60	7:3	Near	30
S3	160	40	4:1	Near	30
S4	180	20	9:1	Near	30
S5	80	120	2:3	Far	30
S6	60	140	3:7	Far	30
S7	40	160	1:4	Far	30
S8	20	180	1:9	Far	30

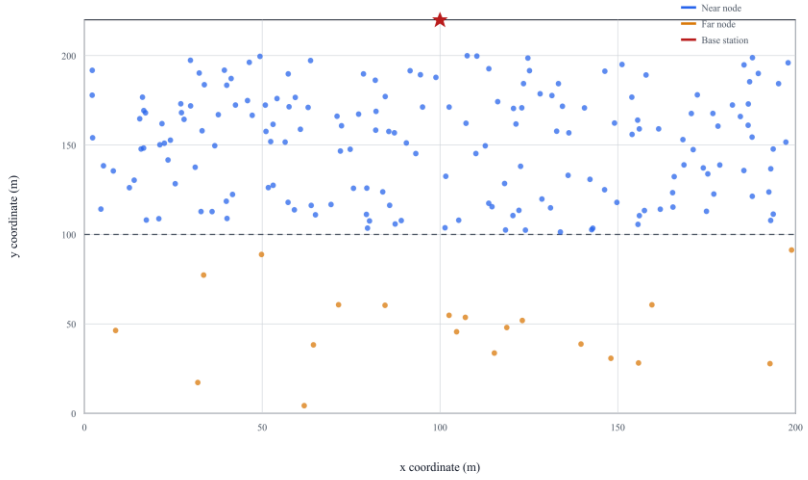


Figure 2. S4_R01 topology and node zones.

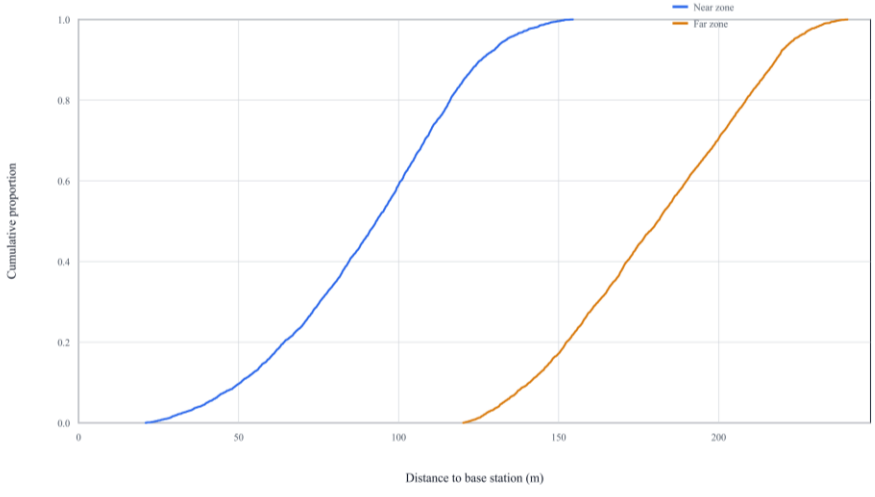


Figure 3. Base-station distance by zone.

Protocol definitions, partition scope, and energy accounting

M1 implements contextual LEACH with p = 0.05, a 20-round eligibility epoch, advertisement (ADV), join, and schedule control phases, nearest active-head membership, and 20 data frames per logical round [2]. It is not the primary causal comparator because it changes both election/formation mechanics and control accounting relative to M2/M3.

For M2/M3, every live node first transmits a 200-bit status message to the base station. Residual energy E_i(r) used for M3 selection is therefore measured after that status debit and before assignment reception or data traffic. Each round initializes 16 particles with one [0,1] coordinate per live node. The ten largest coordinates are distinct seeds; every live node maps to its nearest seed. Velocities use w = 0.7, c1 = c2 = 1.4, and clipping to ±0.2 for 20 iterations [4], [7], [26]. M2 retains the PSO seed as the cluster head. M3 applies the residual-energy rule only after that membership has been selected; exact maximum-energy ties use predicted cluster communication cost and then node ID:

$$CH_k(r) = \arg\max_{i \in C_k(r)} E_i(r) \tag{1}$$

Candidate partition fitness always treats the seed as the temporary head. Let H = 200 control bits, B = 4,200 data bits, P = 4,000 payload bits, and T = 20 frames. The pending member and head costs are:

$$c_i(r) = E_{RX}(H) + T\,E_{TX}(B, d_{i,h}) \tag{2}$$

$$c_h(r) = E_{RX}(H) + T\,(|C_k| - 1)\,E_{RX}(B) + T\,|C_k|\,E_{DA}(P) + T\,E_{TX}(B, d_{h,BS})$$

The PSO objective is evaluated from those common seed-based costs, so M3 reassignment cannot change candidate fitness, seed choice, or membership in the same logical round:

$$J(r) = 0.7\,\max_{i \in A(r)} [c_i(r)/E_0] + 0.3\,\mathrm{mean}_{i \in A(r)} [c_i(r)/E_0] \tag{3}$$

PSO randomness is deterministically derived from the topology-specific protocol seed, logical round, and ordered live-node IDs. Thus, whenever M2 and M3 have the same live set in a round, they receive the same candidate partitions; their live sets can differ after earlier head choices. “Frozen” means that configuration, inputs, seeds, traffic, radio constants, stopping rule, and analysis plan were prespecified—not that memberships are fixed across all rounds or both trajectories.

For L transmitted bits over distance d, the simulator uses the first-order thresholded radio model associated with LEACH and energy-aware WSN communication work [2], [20]–[23], [25]:

$$d_0 = sqrt(\varepsilon_{fs}/\varepsilon_{mp}) \tag{4}$$

$$E_{TX}(L, d) = L\,E_{elec} + L\,\varepsilon_{fs} d^2, d < d_0$$

$$E_{TX}(L, d) = L\,E_{elec} + L\,\varepsilon_{mp} d^4, d \geq d_0$$

$$E_{RX}(L) = L\,E_{elec};\; E_{agg}(L) = L\,E_{DA}$$

Constants were E_elec = 50 nJ/bit, epsilon_fs = 10 pJ/bit/m², epsilon_mp = 1.3×10^{-15} J/bit/m⁴, and E_DA = 5 nJ/bit/signal; d0 = 87.706 m is an energy crossover, not a communication-range limit. Sensor batteries are charged for M2/M3 status transmission, assignment reception, member-to-head transmission, head reception/aggregation, head-to-base-station transmission, and direct-to-base-station fallback. Base-station reception, base-station assignment transmission, and PSO computation are not charged to sensors. The simulator contains no multi-hop relay protocol.

Algorithm 1. M2/M3 round procedure and the isolated M3 intervention.

Step	Procedure
1	Transmit 200-bit status from each live node to the base station; retain nodes with positive residual energy.
2	If fewer than K = 10 nodes remain, apply the direct-to-base-station fallback for each of 20 frames; otherwise continue.
3	Initialize 16 PSO particles with one [0,1] coordinate per live node; update for 20 iterations (w = 0.7, c1 = c2 = 1.4, $\|v\| \leq 0.2$).

Step	Procedure
4	Decode the ten largest particle coordinates as seeds; map every live node to its nearest seed. Score candidate partitions using seed-as-head costs c_i and c_h.
5	M2 retains each seed as cluster head. M3 holds that membership fixed for the logical round and chooses the member with maximum post-status residual energy; ties use predicted cluster cost, then node ID.
6	Charge 200-bit assignment reception, execute member-to-head transmission, head reception/aggregation, and head-to-base-station transmission for 20 frames; use direct fallback after head loss.
7	Update the energy ledger and live set; stop at HND or the 500-round cap, then retain the paired M3−M2 endpoint contrast.

Outcomes, inference, and reproducibility

Let D(r) be the number of depleted nodes by round r and N0 = 200. The prespecified endpoints, which are standard simulation lifetime indicators rather than a claim of complete depletion, were [31]:

$$FND = \min_{\{r:\, D(r) \geq 1\}} \tag{5}$$

$$HND = min\{\, r : D(r) \geq \lceil N_0/2 \rceil \}$$

For scenario s, matched placement j, and endpoint L, the primary estimator was:

$$d_{s,j}^{(L)} = L_{M3,s,j} - L_{M2,s,j} \tag{6}$$

$$\bar{d}_s^{(L)} = (1/30)\, \Sigma_{j=1}\, d_{s,j}^{(L)}$$

Each scenario interval resampled its 30 paired differences 10,000 times [19]. The aggregate block bootstrap resampled placement IDs R01--R30 across all nine scenarios, preserving every scenario-specific contrast within each selected block and hence equal scenario weighting. The two-sided sign-flip statistic was |mean(d)| with 20,000 sign vectors; zero differences remained zero and the plus-one p value was (1+B)/20,001. The fixed random seed was 20261104. Holm adjustment covered the 18 scenario-by-endpoint tests [18]. M1 is contextual; M2 is the primary comparator. Runs stopped at HND or the 500-round cap, so last-node death was neither observable nor reported. Administrative-cap endpoints would have been right-censored and displayed with Kaplan--Meier methods [17].

The executable Python/NumPy implementation retained the frozen configuration, topology-specific seeds, run-level paired outcomes, energy traces, and cluster-selection logs. The supplied archive [32] identifies the topology inputs, not outcome data. These study materials are available from the corresponding author on reasonable request; no public repository identifier is asserted in this manuscript.

3. Results

Execution integrity and descriptive outcomes

All 810 expected runs completed. The maximum absolute energy-ledger closure error was 1.499e-10 J; all 107,550 final M3 maximum-residual-energy checks passed; and 2,377 rounds with equal M2/M3 live sets had matching seed-based partitions. No FND or HND endpoint was censored. Table 3 reports descriptive method outcomes; only M3−M2 isolates the post-partition rule.

Table 3. Method-level lifetime outcomes across 270 topologies per method.

Method	Runs	Mean FND	Mean HND	FND observed	HND observed
M1	270	9.56	34.56	100%	100%
M2	270	8.84	32.84	100%	100%
M3	270	18.70	39.85	100%	100%

M3 mean FND/HND was 18.70/39.85 rounds, versus 8.84/32.84 for M2. Across all matched topologies, M3 had higher/equal/lower FND in 256/5/9 pairs and higher/equal/lower HND in 269/1/0 pairs.

Scenario-stratified primary comparison

Table 4. Primary paired M3−M2 effects by density scenario. Values are mean differences in rounds with 95% percentile bootstrap intervals from 10,000 within-scenario paired resamples.

Scenario	FND M3−M2, rounds [95% CI]	HND M3−M2, rounds [95% CI]
S0	+11.10 [10.37, 11.90]	+7.93 [7.27, 8.60]
S1	+10.13 [9.00, 11.07]	+7.23 [6.63, 7.80]
S2	+9.17 [7.93, 10.33]	+6.03 [5.67, 6.40]
S3	+7.17 [5.57, 8.73]	+3.63 [3.23, 4.00]
S4	+3.73 [2.10, 5.40]	+2.30 [1.93, 2.67]
S5	+11.00 [10.23, 11.80]	+8.27 [7.70, 8.80]
S6	+12.00 [11.13, 12.87]	+9.03 [8.47, 9.60]
S7	+12.10 [11.27, 12.90]	+9.27 [8.80, 9.73]
S8	+12.30 [11.40, 13.10]	+9.40 [9.00, 9.80]

Scenario mean FND effects ranged from +3.73 rounds in S4 to +12.30 in S8; HND effects ranged from +2.30 in S4 to +9.40 in S8. The fixed-resolution unadjusted sign-flip p values were 0.00005, 0.00020; Holm adjustment was applied over all 18 tests. FND lower-than-M2 pairs occurred in scenarios S1, S3, S4, and FND ties occurred in S3, S4; No HND lower-than-M2 pairs occurred, and HND ties occurred in S4.

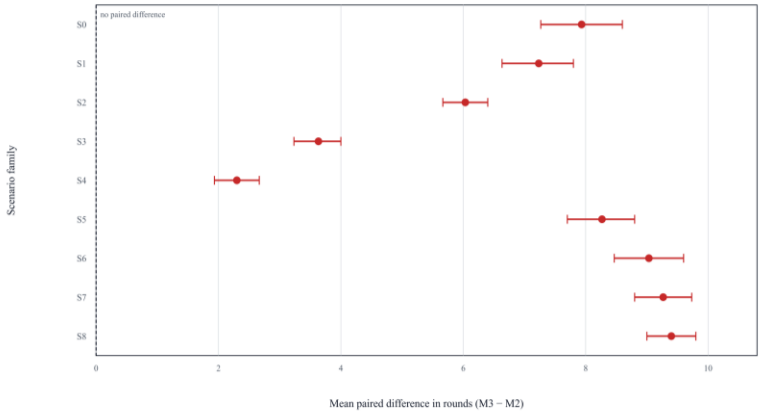


Figure 4. HND gain by scenario.

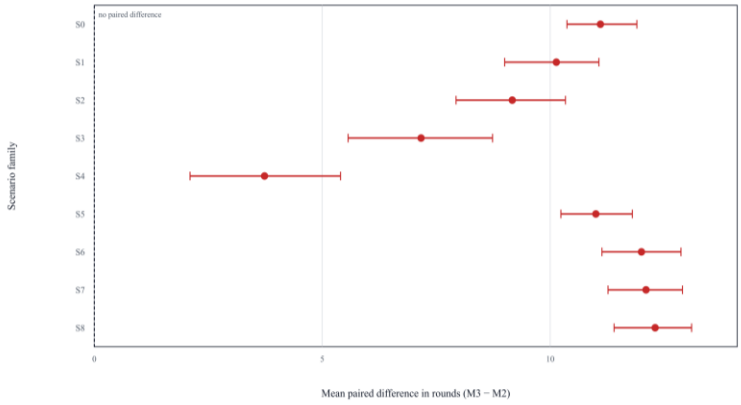


Figure 5. FND gain by scenario.

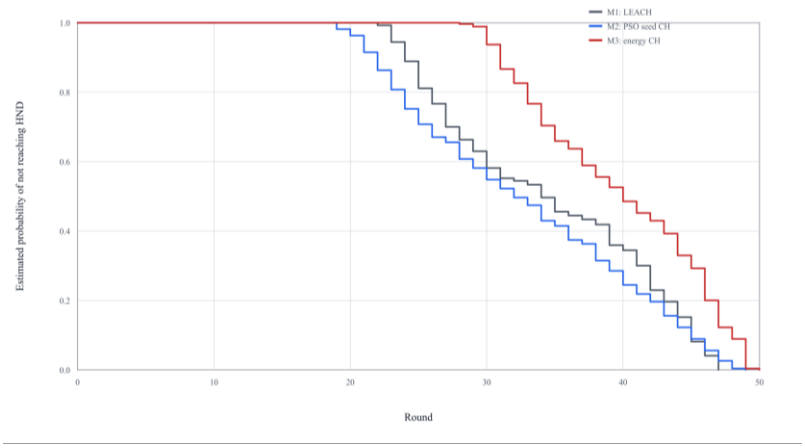


Figure 6. HND survival by method.

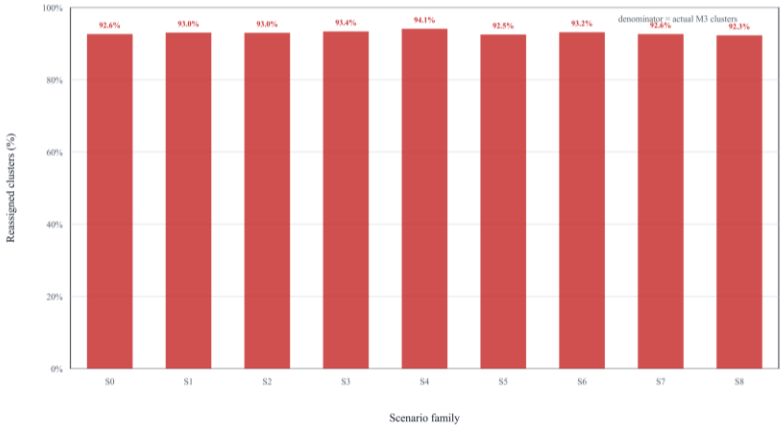


Figure 7. M3 head reassignment by scenario.

Figure 8 combines complementary initial-round M3 samples: S4_R01 has 180 near and 20 far nodes, whereas S8_R02 has 20 near and 180 far nodes. Both show all ten selected M3 heads differing from their PSO seeds; the shared legend and matched axes support direct visual comparison. These are descriptive snapshots, not aggregate performance estimates.

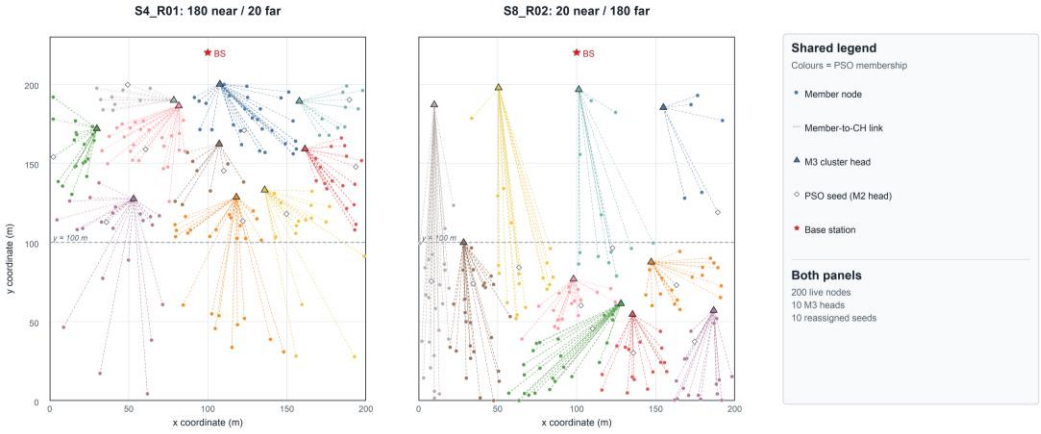


Figure 8. M3 cluster-head samples for S4_R01 and S8_R02.

Discussion

Within the frozen synthetic model, post-partition residual-energy head reassignment improved the aggregate FND and HND estimates relative to retaining the PSO seed. This is a narrow M3−M2 finding: it shares a topology input, deterministic per-state PSO partition, radio model, traffic model, and stopping rule, but does not establish that PSO is generally superior to LEACH or that M3 will improve a deployed WSN.

The scenario results should be interpreted as spatial-distribution effects, not density scaling. Total population and field area remain fixed; changing the near:far split changes the geometry of member-to-head and head-to-base-station distances under the modeled radio cost. FND and HND answer different questions: the earliest exhausted node can respond differently from the point at which half the network is depleted. The observed scenario-specific signs and the exceptions stated above therefore belong to this specified energy ledger. They should not be generalized as a monotone "higher density" effect or as evidence of scalability. The model has no multi-hop relay; its relevant costly operations are member-to-head transmission, head reception/aggregation, head-to-base-station transmission, and direct fallback.

The study also makes a bounded mechanism check possible. The cluster-selection log shows that M3 reassigned 93.0% of final seed clusters, and the invariant confirms the selected node had the maximum eligible residual energy. That supports implementation fidelity, whereas the explanation of why an individual scenario gains more remains model-based: the present traces do not measure fading, interference, retransmission, hardware current draw, or application workload.

Limitations remain material. The input is synthetic and the first-order radio model omits fading, collisions, packet loss, retransmission, hardware variation, security cost, mobility, and spatial correlation beyond the supplied placement process. The objective predicts a fixed pending-frame workload. The endpoints stop at HND/cap, so this study neither observes nor claims full network depletion. Future work should preserve the isolated head-rule contrast while introducing stochastic links, heterogeneous hardware, workload variation, and physical deployments.

4. Conclusion

Across 270 topology-paired synthetic simulations, M3 selected the maximum-residual-energy member after a seed-based PSO partition and achieved aggregate M3−M2 effects of 9.86 FND rounds and 7.01 HND rounds. The conclusion is limited to the frozen model, fixed N = 200 spatial scenarios, and FND/HND endpoints; it does not claim scalability, complete depletion, or field lifetime. The next test is the same controlled comparison under less idealized links and hardware.

References:

[1] I. Akyildiz, Weilian Su, Y. Sankarasubramaniam, E. Cayirci, "A survey on sensor networks," IEEE Communications Magazine, vol. 40, no. 8, pp. 102-114, 2002, doi: https://doi.org/10.1109/MCOM.2002.1024422.

[2] W. Heinzelman, A. Chandrakasan, H. Balakrishnan, "An application-specific protocol architecture for wireless microsensor networks," IEEE Transactions on Wireless Communications, vol. 1, no. 4, pp. 660-670, 2002, doi: https://doi.org/10.1109/TWC.2002.804190.

[3] O. Younis, S. Fahmy, "HEED: a hybrid, energy-efficient, distributed clustering approach for ad hoc sensor networks," IEEE Transactions on Mobile Computing, vol. 3, no. 4, pp. 366-379, 2004, doi: https://doi.org/10.1109/TMC.2004.41.

[4] J. Kennedy, R. Eberhart, "Particle swarm optimization," in Proceedings of ICNN'95 - International Conference on Neural Networks, vol. 4, pp. 1942-1948, 1995, doi: https://doi.org/10.1109/ICNN.1995.488968.

[5] S. Lindsey, C. Raghavendra, "PEGASIS: Power-efficient gathering in sensor information systems," in Proceedings, IEEE Aerospace Conference, vol. 3, pp. 3-1125-3-1130, 2002, doi: https://doi.org/10.1109/AERO.2002.1035242.

[6] L. Qing, Q. Zhu, M. Wang, "Design of a distributed energy-efficient clustering algorithm for heterogeneous wireless sensor networks," Computer Communications, vol. 29, no. 12, pp. 2230-2237, 2006, doi: https://doi.org/10.1016/j.comcom.2006.02.017.

[7] T. SHIH, "Particle Swarm Optimization Algorithm for Energy-Efficient Cluster-Based Sensor Networks," IEICE Transactions on Fundamentals of Electronics, Communications and Computer Sciences, vol. E89-A, no. 7, pp. 1950-1958, 2006, doi: https://doi.org/10.1093/ietfec/e89-a.7.1950.

[8] R. Kulkarni, G. Venayagamoorthy, "Particle Swarm Optimization in Wireless-Sensor Networks: A Brief Survey," IEEE Transactions on Systems, Man, and Cybernetics, Part C (Applications and Reviews), vol. 41, no. 2, pp. 262-267, 2011, doi: https://doi.org/10.1109/TSMCC.2010.2054080.

[9] Y. Gu, Q. Wu, N. Rao, "Optimizing Cluster Heads for Energy Efficiency in Large-Scale Heterogeneous Wireless Sensor Networks," International Journal of Distributed Sensor Networks, vol. 6, no. 1, pp. 961591, 2010, doi: https://doi.org/10.1155/2010/961591.

[10] N. Merabtine, D. Djenouri, D. Zegour, "Towards Energy Efficient Clustering in Wireless Sensor Networks: A Comprehensive Review," IEEE Access, vol. 9, pp. 92688-92705, 2021, doi: https://doi.org/10.1109/ACCESS.2021.3092509.

[11] T. Behera, S. Mohapatra, U. Samal, M. Khan, M. Daneshmand, A. Gandomi, "Residual Energy-Based Cluster-Head Selection in WSNs for IoT Application," IEEE Internet of Things Journal, vol. 6, no. 3, pp. 5132-5139, 2019, doi: https://doi.org/10.1109/JIOT.2019.2897119.

[12] J. Lee, S. Chim, H. Park, "Energy-Efficient Cluster-Head Selection for Wireless Sensor Networks Using Sampling-Based Spider Monkey Optimization," Sensors, vol. 19, no. 23, pp. 5281, 2019, doi: https://doi.org/10.3390/s19235281.

[13] F. Hamzeloei, M. Dermany, "A TOPSIS Based Cluster Head Selection for Wireless Sensor Network," Procedia Computer Science, vol. 98, pp. 8-15, 2016, doi: https://doi.org/10.1016/j.procs.2016.09.005.

[14] Lalit Kumar Tyagi, A. Kumar, "OEE-WCRD: Optimizing Energy Efficiency in Wireless Sensor Networks through Cluster Head Selection Using Residual Energy and Distance Metrics," ICST Transactions on Scalable Information Systems, vol. 11, no. 5, 2024, doi: https://doi.org/10.4108/eetsis.4268.

[15] A. Jalili, M. Gheisari, J. Alzubi, C. Fernández-Campusano, F. Kamalov, S. Moussa, "A novel model for efficient cluster head selection in mobile WSNs using residual energy and neural networks," Measurement: Sensors, vol. 33, pp. 101144, 2024, doi: https://doi.org/10.1016/j.measen.2024.101144.

[16] M. Eskandarpour, S. Pirahmadian, P. Soltani, H. Soleimani, "A Game-Theoretic Reinforcement Learning Approach to Energy-Balanced Cluster-Head Selection in Wireless Sensor Networks," IET Networks, vol. 15, no. 1, 2026, doi: https://doi.org/10.1049/ntw2.70036.

[17] E. Kaplan, P. Meier, "Nonparametric Estimation from Incomplete Observations," Journal of the American Statistical Association, vol. 53, no. 282, pp. 457-481, 1958, doi: https://doi.org/10.1080/01621459.1958.10501452.

[18] S. Holm, "A Simple Sequentially Rejective Multiple Test Procedure," Scandinavian Journal of Statistics, vol. 6, no. 2, pp. 65-70, 1979, [Online]. Available: https://www.jstor.org/stable/4615733. Accessed: 2026-11-04.

[19] B. Efron, "Bootstrap Methods: Another Look at the Jackknife," The Annals of Statistics, vol. 7, no. 1, pp. 1-26, 1979, doi: https://doi.org/10.1214/aos/1176344552.

[20] W. Ye, J. Heidemann, and D. Estrin, "An energy-efficient MAC protocol for wireless sensor networks," in Proc. IEEE INFOCOM 2002, vol. 3, pp. 1567-1576, 2002, doi: https://doi.org/10.1109/INFCOM.2002.1019408.

[21] J. Al-Karaki, A. Kamal, "Routing techniques in wireless sensor networks: a survey," IEEE Wireless Communications, vol. 11, no. 6, pp. 6-28, 2004, doi: https://doi.org/10.1109/mwc.2004.1368893.

[22] C. Intanagonwiwat, R. Govindan, D. Estrin, "Directed diffusion," in Proceedings of the 6th annual international conference on Mobile computing and networking, pp. 56-67, 2000, doi: https://doi.org/10.1145/345910.345920.

[23] W. R. Heinzelman, A. Chandrakasan, and H. Balakrishnan, "Energy-efficient communication protocol for wireless microsensor networks," in Proc. 33rd Annu. Hawaii Int. Conf. Syst. Sci. (HICSS), vol. 2, p. 10, 2000, doi: https://doi.org/10.1109/HICSS.2000.926982.

[24] A. A. Abbasi and M. Younis, "A survey on clustering algorithms for wireless sensor networks," Computer Communications, vol. 30, no. 14-15, pp. 2826-2841, 2007, doi: https://doi.org/10.1016/j.comcom.2007.05.024.

[25] G. Anastasi, M. Conti, M. Di Francesco, and A. Passarella, "Energy conservation in wireless sensor networks: A survey," Ad Hoc Networks, vol. 7, no. 3, pp. 537-568, 2009, doi: https://doi.org/10.1016/j.adhoc.2008.06.003.

[26] N. M. Abdul Latiff, C. C. Tsimenidis, and B. S. Sharif, "Energy-aware clustering for wireless sensor networks using particle swarm optimization," in Proc. 18th IEEE Int. Symp. Personal, Indoor and Mobile Radio Commun. (PIMRC), pp. 1-5, 2007, doi: https://doi.org/10.1109/PIMRC.2007.4394521.

[27] S. Soro and W. B. Heinzelman, “Prolonging the lifetime of wireless sensor networks via unequal clustering,” in Proc. 19th IEEE Int. Parallel and Distributed Processing Symp. (IPDPS), 2005, doi: https://doi.org/10.1109/IPDPS.2005.365.

[28] C. Li, M. Ye, G. Chen, and J. Wu, “An energy-efficient unequal clustering mechanism for wireless sensor networks,” in Proc. IEEE Int. Conf. Mobile Adhoc and Sensor Systems (MASS), pp. 597-604, 2005, doi: https://doi.org/10.1109/MAHSS.2005.1542849.

[29] P. C. S. Rao, P. K. Jana, and H. Banka, “A particle swarm optimization based energy efficient cluster head selection algorithm for wireless sensor networks,” Wireless Networks, vol. 23, no. 7, pp. 2005-2020, 2017, doi: https://doi.org/10.1007/s11276-016-1270-7.

[30] D. Ruan and J. Huang, “A PSO-based uneven dynamic clustering multi-hop routing protocol for wireless sensor networks,” Sensors, vol. 19, no. 8, Art. no. 1835, 2019, doi: https://doi.org/10.3390/s19081835.

[31] I. Dietrich and F. Dressler, “On the lifetime of wireless sensor networks,” ACM Transactions on Sensor Networks, vol. 5, no. 1, Art. no. 5, 39 pp., 2009, doi: https://doi.org/10.1145/1464420.1464425.

[32] “Dataset Simulasi WSN Lifespan v2.0,” Supplied synthetic input package (topologies, generator, and validator), 2026, [Online]. Available: https://wsn-density-benchmark-no7-v1.blackwinggoat.chatgpt.site/downloads/Dataset_Simulasi_WSN_Lifespan_v2.zip.